Available online at website: https://journal.bcrec.id/index.php/bcrec

Bulletin of Chemical Reaction Engineering & Catalysis, 19 (3) 2024, 393-407

Research Article

Optimal Suppression of Photocatalytic Activity of Hybrid TiO_2 Particles in Epoxy Thin Film by Using Taguchi Method

Sunderishwary S. Muniandy‡, Tan Sek Soon‡, Swee-Yong Pung, Sivakumar Ramakrishnan*

School of Materials and Mineral Resources Engineering, Engineering Campus, Universiti Sains Malaysia 14300 Nibong Tebal, Pulau Pinang, Malaysia.

Received: 10th June 2024; Revised: 2nd August 2024; Accepted: 4th August 2024
Available online: 7th August 2024; Published regularly: October 2024

Abstract

In this study, two different Al_2O_3-TiO_2 and SiO_2-TiO_2 hybrid TiO_2 particles were synthesised by using silica (SiO_2) and alumina (Al_2O_3) to suppress the photocatalysis of TiO_2. Key variables such as the concentration of the hybridization material (C), heating temperature (T_h), and calcinating temperature (T_c) were selected with performance measured by photodegradation rate. The Taguchi L_9 orthogonal array, a systematic approach used in the design of experiments (DOE), confirmed A333 (Al_2O_3-TiO_2) achieved 99% photodegradation suppression with photodegradation rate reduced significantly from 0.01305 min^{-1} to 0.00009 min^{-1} and improved yellowing resistance by 63%, while S323 (SiO_2-TiO_2) achieved 75% suppression with photocatalysis activity decreased from 0.01305 min^{-1} to 0.0033 min^{-1} and 42% improved resistance. X-ray Diffraction (XRD) analysis showed A333 had a higher rutile phase (40.1% vs. 10.2% for S323), and Fourier Transform Infra Red (FTIR) and Field Emission Scanning Electron Microscopy (FESEM) analyses revealed A333's rougher surface and lower surface area compared to S323 and pure TiO_2. Overall, A333 effectively suppressed photocatalysis and improved yellowing resistance of epoxy thin film.

Keywords: TiO_2; hybrid particles; Al_2O_3-TiO_2; SiO_2-TiO_2; suppression of photocatalytic activity; Taguchi method; epoxy; yellowing

How to Cite: S.S. Muniandy, T.S. Soon, S.-Y. Pung, S. Ramakrishnan (2024). Optimal Suppression of Photocatalytic Activity of Hybrid TiO_2 Particles in Epoxy Thin Film by Using Taguchi Method. *Bulletin of Chemical Reaction Engineering & Catalysis*, 19(3), 393-407 (doi: 10.9767/bcrec.20164)

1. Introduction

TiO_2 is an excellent photocatalyst that possesses high photocatalytic activity, non-toxicity, high stability within a wide range of pH, low cost, and fast electron transfer to molecular oxygen [1]. TiO_2 has been widely used in a variety of consumer and industrial applications for decades, such as colorant in substances, cosmetics, water treatment, the pharmaceutical industry, electrochemical electrodes, capacitors, solar cells, food additives, and toothpaste [2]. TiO_2 also can act as a colorant as it scatters visible light to whiten the surrounding substances due to its high refractive index and it can increase the refractive index of polymeric materials to increase the transmittance of light where it can be useful for optical applications such as light emitting diode (LED) encapsulants [3]. According to Huang *et al.* [4] incorporating TiO_2 into a LED encapsulant could improve the properties and efficiency of LEDs by increasing the refractive index of the encapsulant. Also, by incorporating TiO_2 particles in the encapsulant, it increases the thermal conductivity, therefore improving the thermal stability and the reliability of the LED [5].

However, one of the common problems encountered by the LED industry by using TiO_2 as the filler is the performance of LEDs could deteriorate from reliability problems such as polymeric encapsulant discoloration. This is because since TiO_2 has a wide band gap (3.2 eV), it absorbs UV light where the free radicals with high reactivity will be produced from the photocatalysis process. When free radicals encounter the polymeric fillers, they can initiate a

* Corresponding Author.
Email: srsivakumar@usm.my (S. Ramakrishnan)
‡ Both authors contributed equally to this manuscript.

chain reaction that breaks down the molecular structure of the polymeric compound which can lead to a loss of its physical and mechanical properties [6–8]. This process is known as photodegradation. Besides, free radicals can react with oxygen in the air, creating peroxide and other reactive species that can lead to discolouration, embrittlement, and cracking of the polymeric material in the LED [9]. Consequently, the suppression of the photocatalytic activity of TiO_2 is believed to be able to inhibit the generation of free radicals that will degrade the surrounding organic compound, which eventually will improve the performance of LED in the long run.

Suppression of the photodegradation can be achieved *via* modification on TiO_2 particles in the polymeric materials. The most common polymeric materials used in the making of the encapsulant are silicone and epoxy [8]. Silicone possesses superior optical and thermal properties while epoxy resin has a lower price, stronger mechanical properties, longer lifetime, and weaker UV-aging resistance [10]. With a good combination of ease of manufacturing, mechanical stabilities, and UV resistance, the modified epoxy could become more useful in applications involving LED encapsulants. Hence, TiO_2 could be hybridized by many materials to alter its photocatalytic performance. Optical transparency and its insulating properties inhibit the transportation of electrons and holes [11], which suppress the formation of free radicals. Hybrid TiO_2 particles exhibit well-planned physicochemical characteristics as a result of fusing the distinctive behaviors of the constituent chemicals. The structural, textural, acid/base, and catalytic properties of pure TiO_2 particles could be significantly impacted by the addition of an external element [12].

TiO_2 could be hybridized by many materials such as SiO_2, Al_2O_3, chitosan, graphene oxide, hematite, and carbon to alter its photocatalytic performance [13–18]. A significant impact on the degradation efficiency to the TiO_2 particles through the incorporation of SiO_2 and Al_2O_3 has been discovered due to their optical transparency and their insulating properties to inhibit the transportation of electrons and holes [11]. Besides, the wide bandgap of SiO_2 (7.62– 9.70 eV) and Al_2O_3 (7.0–7.6 eV) [19–21] is believed to be able to widen the bandgap of TiO_2, which could inhibit the migration of photogenerated charged carriers.

This article focuses on developing Al_2O_3-TiO_2 and SiO_2-TiO_2 hybrid particles via sol-gel methods to reduce TiO_2's photocatalytic activity. The Taguchi method can optimize synthesis parameters by minimizing variance and examining factor interactions using orthogonal arrays. The optimal hybrid particles can be incorporated into thin epoxy films to assess their effectiveness in resisting UV-induced discoloration.

2. Material and Method

2.1 Materials

Tetrabutyl orthotitanate, TBT ≥ 97% purity (Fluka Analyticals, Sigma-Aldrich, Co.), Tetraethyl orthosilicate, TEOS 99% purity (Fluka Analyticals, Sigma-Aldrich, Co.), Aluminium Chloride, $AlCl_3$ 99% purity (BDH), Hydrochloric acid, HCl (Merck), Epoxy resin, Rhodamine B (RhB) dye (Merck). All reagents were used as purchased and without further purification.

2.2 Synthesis of Hybrid TiO_2 Particles

The TiO_2 sol was prepared by the hydrolysis of tetrabutyl orthotitanate (TBT) [22,23]. Ethanol was used in a molar ratio of 25:1 relative to the TBT solution. It was added drop by drop into the TBT (10.2267 g, 8.5223 g, and 6.8178 g) under continued stirring for 30 min and 2 mL of hydrochloric acid (HCl) was added drop by drop to the mixture while stirring for an additional 30 min. Hydrolysis was then initiated by adding de-ionized water to the solution and stirring for 2 h. The de-ionized water was added according to a 35:1 molar ratio of de-ionized water to ethanol. The solution was aged overnight to complete all the reactions before it was stirred again for another 1 h. This solution was indicated as Solution A.

In the process of synthesising Al_2O_3-TiO_2, aluminium chloride ($AlCl_3$) was used as the precursor for Al_2O_3 [4]. Selected amounts of $AlCl_3$ (4.1849 g, 5.2311 g, or 6.2773 g) were added into 100 g of deionised water and stirred for 1 h until it was fully dissolved. Then, it was mixed with Solution A and the mixture was heated on the hotplate at (55, 100, and 145 °C) for 1 h, the real-time temperature of the mixture was observed by using the thermoset to ensure the temperature was accurate [23,25]. The precipitates were found at the bottom of the beaker. The mixture was centrifuged at 3000 rpm for 15 min to remove the excess solution and washed by using deionised water 3 times to obtain the precipitates. Next, the precipitates were then dried in the oven for 13 h at 70 °C and cooled to room temperature. The dried sample was sent to the furnace for calcination at different temperatures (700, 800, and 900 °C) with a heating rate of 2.5 °C/min and a soaking time of 1 h [26]. Next, the sample was cooled to room temperature. The final product was ground with ethanol as a grinding medium to obtain the micro and nanoparticles.

The process of synthesising SiO_2-TiO_2 was identical to the above. The only difference was the amount of TBT (16.5332, 16.1923, and 15.8514 g),

replacing $AlCl_3$ with tetraethyl orthosilicate (TEOS) (5.5481, 6.9351, and 8.3221 g), and replacing 100 g of deionised water to 20 ml of ethanol as a solvent for TEOS [27,28]. The pure TiO_2 particles were synthesised by using the synthesis parameters that produced the lowest photocatalytic performance of hybrid TiO_2

2.3 Incorporation of Hybrid TiO_2 Particles into Epoxy Thin Film

For the preparation of the thin epoxy film, 3 g of epoxy resins were first mixed with 1 g of hardener solution. Then, it was mixed with 0.005 g of synthesised hybrid TiO_2 particles in a beaker. The uniform dispersion of the particles was achieved by ultrasonication, then the mixture was transferred to the silicone mould. Finally, the resin was cured in the oven at 40 °C overnight to obtain the thin film. The thin films were cut into half to make a comparison before and after the 5 h of UV irradiation.

2.4 Characterisations

The morphology and elemental evaluation of the hybrid TiO_2 particles were done through field-emission scanning electron microscope (FESEM) (ZEISS SUPRA 35VP) and Energy Dispersive X-Ray spectrophotometer (EDX) analysis. The crystal phase and orientation of the samples were identified by using X-Ray Diffraction (XRD) (Bruker D2 Phaser model) using Cu Kα radiation (0.15406 nm) with a scanning range from 10° to 90° of 2θ at 30 kV. The presence of the chemical bonds in the samples were identified by using FTIR spectroscopy. The zeta potential of the samples were measured by using the Malvern Zetasizer Nano series by dispersing 0.05 g of the sample in 60 ml of ultrapure water via ultrasonication. Zetasizer can identify the stability of particle dispersion, aggregation, or flocculation of the particles. A precise surface area and porosity distribution of solid materials were measured via BET analysis. A degassing procedure is required in BET to eliminate any moisture that may be physically bound to the surface. The degassing procedure is carried out for 8 h in a vacuum condition at 350 °C.

2.5 Evaluation of Photocatalytic Activities

The photocatalytic activities of synthesised hybrid TiO_2 particles (Al_2O_3/TiO_2 and SiO_2/TiO_2) were evaluated using RhB dye as the organic dye. The synthesised sample (0.05 g) was added into the 5 ppm of RhB dye solution. The mixture was then stirred under UV radiation conditions inside a light chamber. The RhB solution with synthesised samples were stirred for 30 min under dark conditions and then exposed to UV irradiation for 90 min. The degradation efficiency of RhB solution was analysed using a UV-Vis spectrometer (Varian Cary 50) with a wavelength range from 800 nm to 400 nm. The rate constant of the photodegradation was presented by using the Pseudo-First-Order Kinetic Model and the photodegradation efficiencies of the samples were calculated by Equation (1) as follows:

$$E = \frac{C_0 - C}{C_0} \times 100\% \quad (1)$$

Table 1. Synthesis parameters of Al_2O_3/TiO_2 and SiO_2/TiO_2.

Symbol	Process parameters	Units	Levels		
			1	2	3
C	Concentrations	mol%	40	50	60
T_h	Heating temperature	°C	55	100	145
T_c	Calcinating temperature	°C	700	800	900

Table 2. Experimental plan of the Taguchi method for Al_2O_3-TiO_2 and SiO_2-TiO_2.

Al_2O_3-TiO_2	SiO_2-TiO_2	Experiment runs	Controllable synthesis parameters		
			C (mol%)	T_h (°C)	T_c (°C)
A111	S111	1	1	1	1
A122	S122	2	1	2	2
A133	S133	3	1	3	3
A212	S212	4	2	1	2
A223	S223	5	2	2	3
A231	S231	6	2	3	1
A313	S313	7	3	1	3
A321	S321	8	3	2	1
A332	S332	9	3	3	2

where, C_0 and C represent the solution concentration or absorbance before and after degradation, respectively.

2.6 The Taguchi Method

The Taguchi statistical method is employed to look at how different parameters affect the mean and variance of a process. The Taguchi method uses the mixed-level fractional factorial designs to conduct the fewest experiments feasible while staying within the parameters of the factors and levels permitted. In this research, the Taguchi statistical method is used to optimise the synthesis parameters to suppress the photocatalytic activity of hybrid TiO_2. The synthesis process has 3 factors with 3 levels each. Table 1 shows the range of each controllable variable and their levels for synthesizing hybrid TiO_2 particles using Al_2O_3 and SiO_2.

The design of the Taguchi method was a Taguchi L_9 orthogonal array for performing the experiments. The design of L_9 orthogonal array is shown in Table 2 [29]. It was applied to both synthesis processes of Al_2O_3-TiO_2 and SiO_2-TiO_2.

After conducting the experiments, the rate of photodegradation of each sample was obtained to measure the signal-to-noise (S/N) values of the process. Then, the confirmation test was carried out by comparing the experimental S/N ratio of the sample synthesised via the optimum parameter and its predicted S/N ratio [30]. S/N calculations were further elaborated in the section 3.3.

2.7 Evaluation of the Yellowing of Epoxy Film

The epoxy thin films incorporated with optimum hybrid TiO_2 particles (Al_2O_3/TiO_2 and SiO_2/TiO_2) obtained from the confirmation test of the Taguchi method were inserted into the UV chamber to be irradiated by the UV light for 5 h to study the effect of hybrid TiO_2 particles on the resistance of epoxy film towards UV radiation. The yellowness index of the thin films was calculated to study the degree of yellowness. The degree of yellowing was measured by using the Yellowness Color index measurement of standard Tristimulus values according to the International Commission on Illumination (CIE) to measure the RGB (Red, Green, Blue) value of the epoxy film. The calculation of RGB values was further discussed in section 3.4.

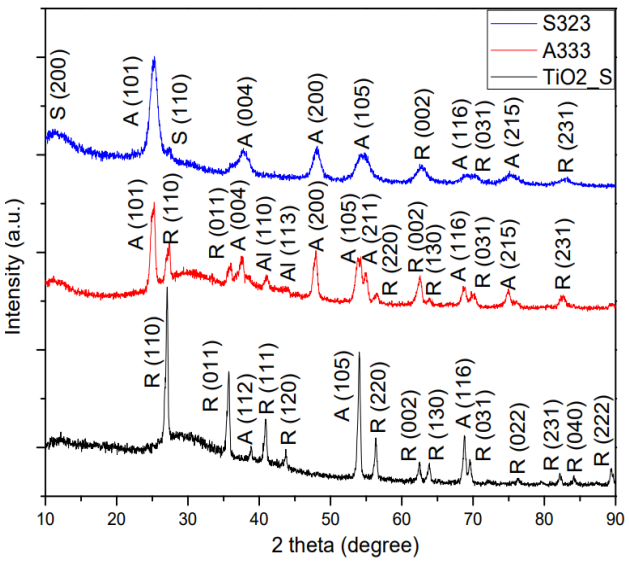

Figure 1. XRD patterns of pure TiO_2, A333 and S323.

3. Results and Discussion

3.1 Characterization of Hybrid TiO_2

3.1.1 XRD analysis

Figure 1 illustrates the X-ray diffraction (XRD) patterns of pure TiO_2 particles and the hybrid TiO_2 particles with optimum synthesis parameters (A333 and S323). For the pure TiO_2, the diffraction peaks at 2θ = 27.477°, 36.138°, 41.306°, 44.111°, 56.716°, 62.870°, 64.152°, 69.121°, 76.679°, 82.485°, 84.401°, and 89.725° correspond to (110), (011), (111), (120), (220), (002), (130), (031), (022), (231), (040), and (222) tetragonal rutile phase of TiO_2 (ICSD 98-004-6226). The peaks at 2θ = 38.314°, 53.344°, and 68.052° correspond to (112), (105), and (116) tetragonal anatase phase of TiO_2 (ICSD 96-900-8217). For A333, the peaks at 2θ = 25.156°, 37.385°, 47.782°, 53.344°, 54.752°, 68.052°, and 74.397° correspond to (101), (004), (200), (105), (211), (116), and (215) tetragonal anatase phase of TiO_2 (ICSD 96-900-8217). The peaks at 2θ = 27.477°, 36.138°, 56.716°, 62.870°, 64.152°, 69.121°, and 82.458° correspond to (110), (011), (220), (002), (130), (031), and (231) tetragonal rutile phase of TiO_2 (ICSD 98-004-6226). For S323, the peaks at 2θ = 25.156°, 37.385°, 47.782°, 53.344°, 68.052°, and 74.397° correspond to (101), (004), (200), (105), (116), and (215) tetragonal anatase phase of TiO_2 (ICSD 96-900-8217). The peaks at 2θ = 5.697° and 27.404° correspond to (200) and (110) tetragonal cristobalite phase of SiO_2 (ICSD 96-901-6250). The peaks at 2θ = 62.870°, 69.121°, and 82.485° correspond to (002), (031), and (231) tetragonal rutile phase of TiO_2 (ICSD 98-004-6226). In addition, the Rietveld refinement was carried out to study the percentage of phases in A333 and S323. A333 has a higher rutile percentage (40.1% vs 10.2%) and lower anatase percentage (36.5% vs 71.6) than S323. The higher percentage of the rutile phase has contributed to the better suppression of A333 than S323 because rutile is a weaker phase of TiO_2 in terms of photocatalytic activity [31].

3.1.2 FTIR analysis

Figure 2 demonstrates the FTIR spectrum of pure TiO_2 particles and the hybrid TiO_2 particles with optimum synthesis parameters (A333 and S323). The peak at 510 cm^{-1} for all samples corresponds to the Ti–O vibration [32], which confirms the presence of the TiO_2 particles in the sample. For pure TiO_2, the peaks at 451 cm^{-1} correspond to the stretching vibrations mode of the Ti–O [33]. For A333, the peaks at 433 cm^{-1}, 1130 cm^{-1}, 1355 cm^{-1}, 1722 cm^{-1}, and 3618 cm^{-1} correspond to the stretching vibrations mode of the Al–O, Al–O–H, Al=O, Ti–OH, and –OH bond bands, respectively [32,34,35]. For S323, the peaks at 790 cm^{-1}, 970 cm^{-1}, 1072 cm^{-1}, 1620 cm^{-1}, and 3721 cm^{-1} correspond to the stretching vibrations mode of the Si–O–Si, Si–OH, Si–O–Si, –OH, and Si–OH bond bands, respectively [32,33,36].

3.1.3 FESEM and EDX analysis

Figure 3 shows the FESEM image and EDX results of pure TiO_2, A333, and S323. The surface morphology of the samples was observed under the magnification of 30kX via FESEM. The pure TiO_2 particles appeared to be spherical shapes, while the particles of A333 and S323 appeared to be irregular shapes. The pure TiO_2 particles tended to agglomerate and formed the micro-size particles, while the smaller particles in A333 and S323 tended to adhere to the larger particles due to the weak stability of the particles that caused aggregation. The agglomeration and aggregation of the particles were due to the adhesion of the particles to each other by weak forces, which reduced the surface area of the particles [37]. The surface of the S323 appeared to be less rough than A323 and pure TiO_2, it indicates that the hybridization of the TiO_2 with SiO_2 could produce a smoother particle surface than Al_2O_3. The surface roughness and the agglomeration of TiO_2 particles could reduce the amount of accessible hydroxyl group (HO•) at the surface of the particles [37]. It could reduce the number of free radicals generated and subsequently reduce the photocatalytic performance of the particles. The EDX results show that pure TiO_2 has 61.73% and 38.27% atomic percentage of O and Ti, respectively, which corresponds to the chemical formula of TiO_2. For A333, the atomic percentage

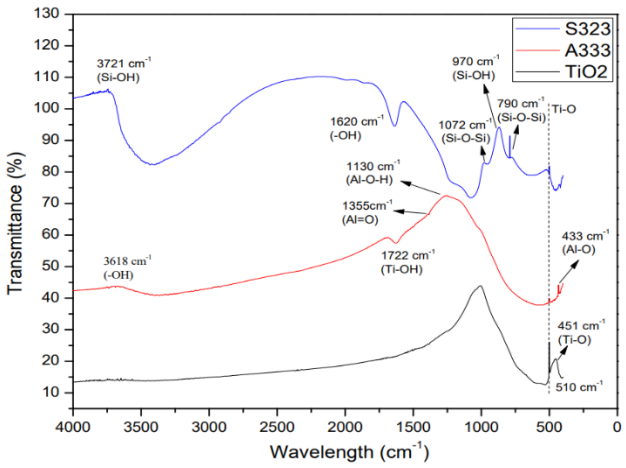

Figure 2. FTIR spectrum of pure TiO_2, A333 and S323

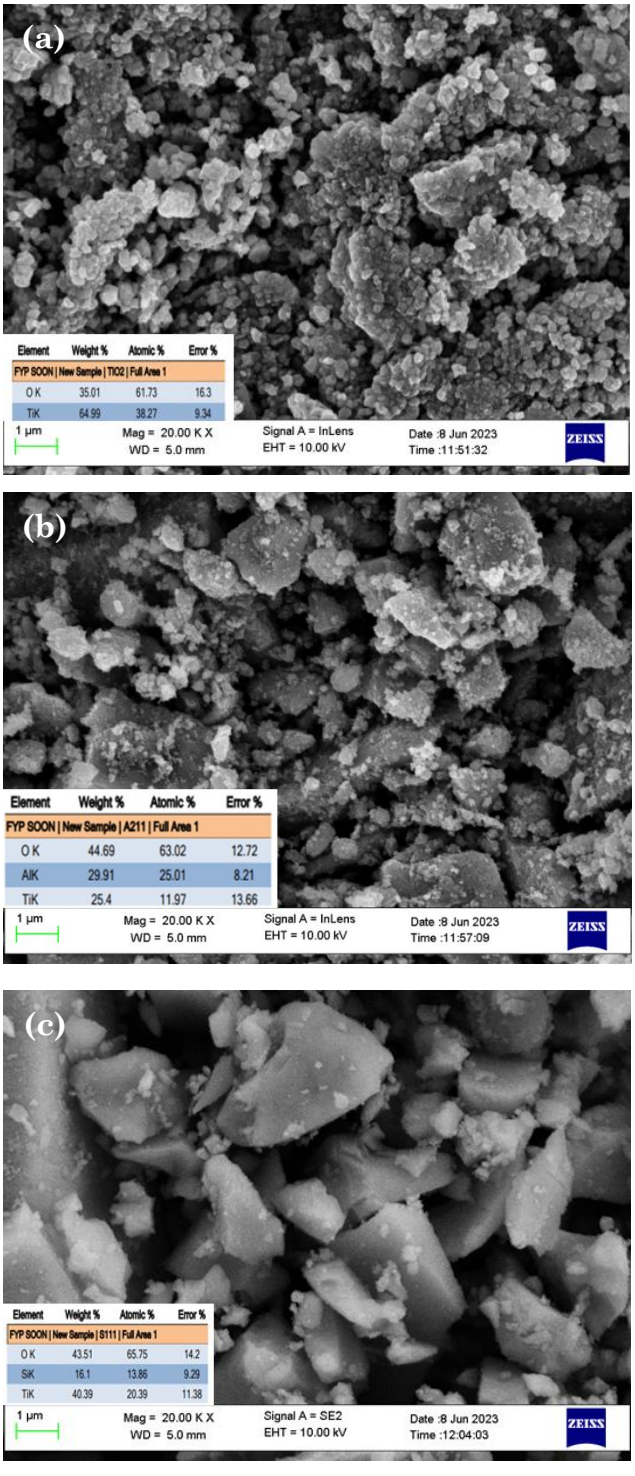

Figure 3. FESEM image and EDX results of (a) pure TiO_2, (b) A333, and (c) S323.

of O, Al, and Ti are 63.02%, 25.01%, and 11.97% respectively. The theoretical atomic percentage of Al in 60 mol% of Al_2O_3 and 40 mol% of TiO_2 is 28.57%, which was close to the experimental atomic percentage of 25.01%. For S323, the atomic percentage of Ti, Si, and O was 65.75%, 13.86%, and 20.39% respectively. The theoretical atomic percentage of Si in 60 mol% of SiO_2 and 40 mol % of TiO_2 is 32.96%, which was different to the experimental atomic percentage of 13.86%. In conclusion, the EDX results have shown that the elemental composition of the samples was close to the theoretical values.

3.1.4 Zeta Potential Analysis

Most of the Al_2O_3-TiO_2 particles have shown positive zeta potential with 16.5 mV to 33.5 mV, while the pure TiO_2 particles, A133, and A333

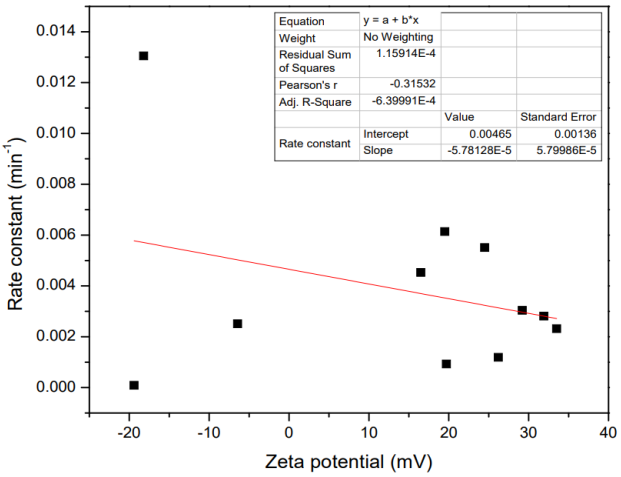

Figure 4. Scatter plot of rate constant vs zeta potential of Al_2O_3-TiO_2 and pure TiO_2 particles.

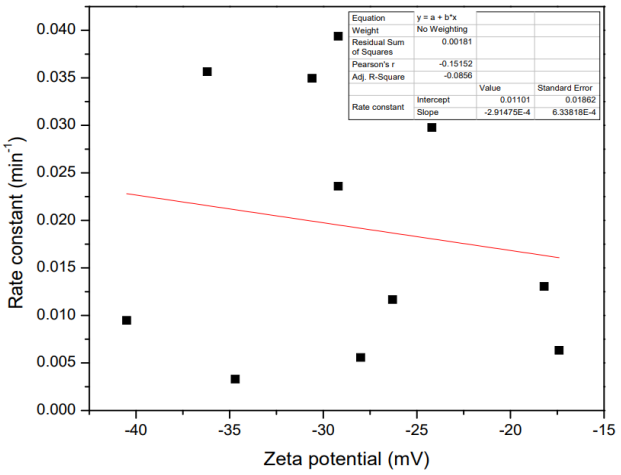

Figure 5. Scatter plot of rate constant vs zeta potential of SiO_2-TiO_2 and pure TiO_2 particles.

Table 3. The average zeta potential of Al_2O_3-TiO_2 and pure TiO_2 produced by different synthesis parameters.

Sample	Zeta potential (mV)	Standard deviation (mV)
A111	19.5	5.56
A122	16.5	4.67
A133	-6.43	7.09
A212	31.9	6.29
A223	26.2	6.76
A231	23.2	7.38
A313	33.5	5.26
A321	24.5	7.30
A332	19.7	10.3
A333	-19.4	5.25
TiO_2_S	-18.2	5.95

Table 4. The average zeta potential of SiO_2-TiO_2 and pure TiO_2 produced by different synthesis.

Sample	Zeta potential (mV)	Standard deviation (mV)
S111	-29.2	5.96
S122	-36.2	6.05
S133	-26.3	4.91
S212	-30.6	4.21
S223	-28.0	5.36
S231	-24.2	4.81
S313	-17.4	5.48
S321	-29.2	5.80
S332	-40.5	6.46
S323	-34.7	5.35
TiO_2_S	-18.2	5.95

have shown negative zeta potential with −18.2 mV, −6.43 mV, and −19.4 mV respectively as shown in Table 3. Also, all SiO_2-TiO_2 particles showed negative zeta potential ranging from −17.4 mV to −40.5 mV can be observed in Table 4. The positive zeta potential indicated the high stability of the particles to resist agglomeration as there was electrostatic repulsion between particles, while the negative zeta potential indicates the low stability of the particles [38]. Figure 4 and Figure 5 shows the scatter plots of rate constant vs zeta potential of the hybrid and pure TiO_2 particles. Pearson's correlation coefficient (*r*) was calculated by using it to show the correlation coefficient between the zeta potential and the rate of photodegradation. The correlation coefficient ranges from -1 to 1, where -1 indicates a strong negative correlation, 0 indicates no correlation, and 1 indicates a strong positive correlation. For Al_2O_3-TiO_2 and SiO_2-TiO_2, Pearson's *r* was -0.31532 and -0.15152 respectively, which indicates that there is a slight negative correlation between the rate constant and zeta potential for the hybrid and pure TiO_2 particles. It could be concluded that the degree of agglomeration of the particles has no significant impact on the rate of photodegradation for the hybrid TiO_2 particles. Similar results were obtained by Tyukavkina *et al*. [17], where the sample had the lowest agglomeration and particle size among all the samples possessed the ability to suppress photocatalytic activity. Therefore, the degree of agglomerations did not have a significant impact on the performance of the photocatalytic activity.

3.1.5 BET Surface Area Analysis

The BET total surface area and the particle size of pure TiO_2, A333 and S323 particles are shown in Table 5. Pure TiO_2 has shown the highest total surface area among all (208.8179 m^2/g), A333 has shown the lowest total surface area among all (5.2067 m^2/g), and S323 has a total surface area of 26.2950 m^2/g. As measured in the previous section, the rate of photodegradation of A333 is the lowest, followed by S323 and pure TiO_2. It was observed that the rate of photodegradation of the particles decreased with the total surface area of the particles. It might be due to a larger number of surface-active sites for the reaction to take place [39]. Normally, the total surface area of the particles will be higher when the particle size is smaller, thus increasing the photocatalytic activity of the photocatalyst [40]. However, the total surface areas of the particles in this study were not affected by the particle size. The particle size of S323 was almost 2 times larger than A333, but the total surface area of S323 was almost 5 times larger than A333. It might be due to the total pore volume of the S323 being larger than A333, which created more total surface area in the particles. Similar results were obtained by Hosseini *et al*. [41], where two particles of similar particle size were observed, but different pore volumes showed different total surface area. Which concluded that the particles with higher pore volume have a higher total surface area. From the BET analysis, it can be concluded that Al_2O_3-TiO_2 and SiO_2-TiO_2 suppressed the photocatalytic activity due to their lower surface area than pure TiO_2.

Table 5. BET surface area analysis of pure TiO_2, A333 and S323 particles.

Sample	Total surface area (m^2/g)	Average particle size (nm)
Pure TiO_2	208.8179	356.6
A333	5.2067	486.4
S323	26.2950	1002

Table 6. Removal efficiency and rate constant of Pseudo-First-Order Kinetic Modelling of Al_2O_3-TiO_2 produced by different synthesis parameters.

Sample	Removal efficiency after 90 min of UV irradiation (%)	Pseudo-First-Order Kinetic Modelling	
		Rate of photodegradation, K_1 (min^{-1})	Coefficient of determination, R^2
A111	**60.76590**	**0.00614**	**0.99682**
A122	34.46239	0.00453	0.99850
A133	20.75167	0.00251	0.99543
A212	20.32839	0.00281	0.98721
A223	10.03197	0.00119	0.99890
A231	24.6665	0.00304	0.99069
A313	18.16928	0.00232	0.99585
A321	39.64129	0.00551	0.99940
A332	**7.496520**	**0.00093**	**0.98906**
TiO_2_S	73.19104	0.01305	0.98607

3.2 Photocatalytic and Kinetic Studies of Hybrid TiO_2

The photocatalytic performance of hybrid TiO_2 particles synthesised using different synthesis parameters in degrading RhB dye solution was studied. Noted that the samples were named after the synthesis parameters, for example, A111 represented by TiO_2 hybridised by Al_2O_3 and was synthesised by the parameters following C_1, T_{h1}, and T_{c1}, where C = concentration of the hybridization materials, T_h = heating temperature, and T_c = calcinating temperature. Table 6 and Table 7 summarise the removal efficiency (%) after 90 min of UV irradiation, the rate of degradation of Pseudo-First-Order Kinetic Modelling (min^{-1}), and the coefficient of determination of Al_2O_3-TiO_2 and SiO_2-TiO_2 hybrid particles.

Figure 6 shows the kinetic plot and the rate of photodegradation of the hybrid TiO_2 particles in RhB dye solution under 90 min of UV irradiation. A332 and S223 achieved the highest removal efficiencies of 60.765% and 98.762%, respectively after 90 min of UV irradiation. They also had a rate of photodegradation of 0.00614 min^{-1} and 0.03938 min^{-1}, respectively. On the other hand, A111 and S111 achieved the lowest removal efficiencies of 7.497% and 37.416%, respectively after 90 min of UV irradiation. They also recorded a rate of photodegradation of 0.00093 min^{-1} and 0.00557 min^{-1}, respectively. When compared to the pure TiO_2 particles with 73.191% removal efficiency and 0.01305 min^{-1} rate of photodegradation, all samples of Al_2O_3-TiO_2 have obtained a lower rate of photodegradation than pure TiO_2.

On the contrary, only 4 samples of SiO_2-TiO_2 obtained a lower rate of photodegradation than pure TiO_2, which were S223, S313, S321, and S332. It was observed that with higher concentrations of SiO_2, the rate of photodegradation would be suppressed. When the concentration of SiO_2 was low, the rate of photodegradation would be enhanced. It could be

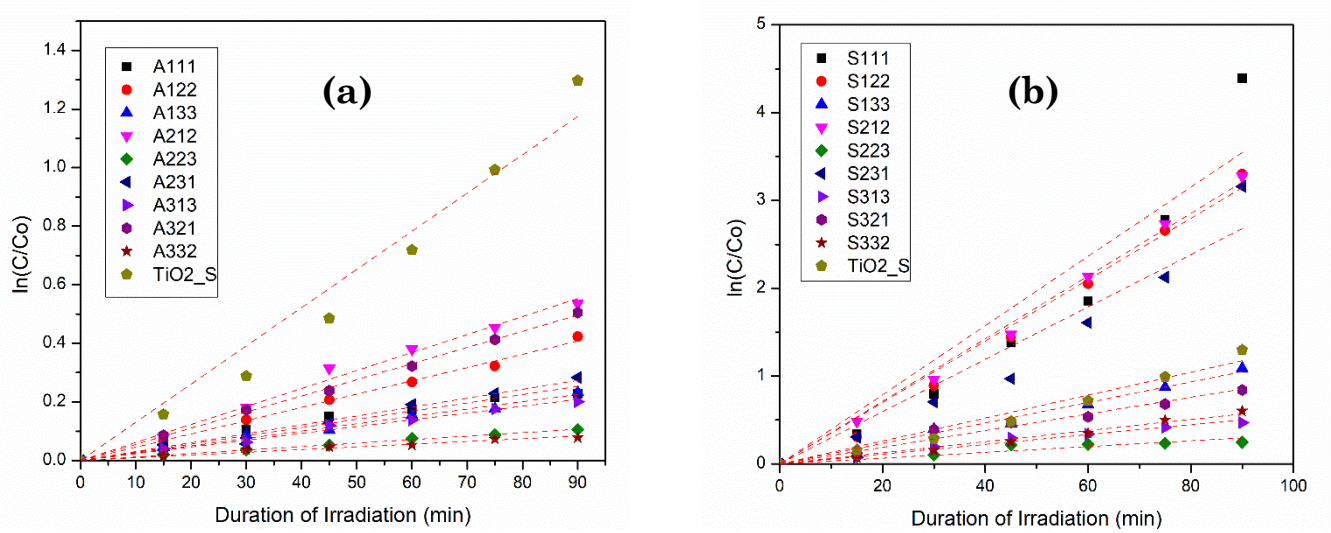

Figure 6. Kinetic plot of Pseudo first order of (a) Al_2O_3-TiO_2 and (b) SiO_2-TiO_2.

Table 7. Removal efficiency and rate constant of Pseudo-First-Order Kinetic Modelling of SiO_2-TiO_2 produced by different synthesis parameters

Sample	Removal efficiency after 90 min of UV irradiation (%)	Pseudo-First-Order Kinetic Modelling	
		Rate of photodegradation, K_1 (min^{-1})	Coefficient of determination, R^2
S111	**98.76284**	**0.03938**	**0.95177**
S122	96.21673	0.03495	0.99467
S133	88.88429	0.02359	0.99584
S212	96.31167	0.03565	0.99828
S223	**37.41583**	**0.00557**	**0.99253**
S231	95.75585	0.02977	0.97082
S313	45.25445	0.00633	0.99194
S321	66.29067	0.01167	0.99624
S332	56.89244	0.00948	0.99028
TiO_2_S	73.19104	0.01305	0.98607

concluded that a smaller amount of SiO_2 could improve the rate of photodegradation while a higher amount of SiO_2 could suppress the rate of photodegradation. For both hybrid particles, the highest rate of degradation was achieved with all the synthesis parameters of level 1, which were 40 mol% of hybridization materials, 55 °C of heating temperature, and 700 °C of calcinating temperature. The high photodegradation rate could be due to the higher amount of the anatase phase resulting from the lower calcinating temperature of 700 °C as shown in Figure 6.

The coefficient of determination is the measure of the goodness of fit (R^2) of a model, which ranges from 0 to 1. A value that is closer to 1 indicates that it has better fits. The R^2 for both tables range from 0.95177 to 0.99940, which indicates all of them have good fitness.

3.3 The Taguchi Method

The optimization of the synthesis parameters of Al_2O_3-TiO_2 and SiO_2-TiO_2 were performed by using the Taguchi Method. The rate of photodegradation of each sample was obtained and converted to the signal-to-noise (S/N) ratios that represented the quality of the product. The S/N ratios were calculated based on the rate of photodegradation of the samples. The ratio of mean to standard deviation is known as the S/N ratio. Taguchi coined the terms "signal" and "noise," which refer to the response's desired value (mean) and undesirable value (standard deviation), respectively. Taguchi categorises the S/N ratio into three groups based on the reaction requirements: medium-the-better, bigger-the-better, and smaller-the-better [30]. In this study, a smaller rate of photodegradation is desirable. The calculation of the S/N value of smaller the better by using Equation (2).

$$S/N \text{ value for smaller the better} = -10\log\left(\frac{1}{n}\right)\sum\left(R^2\right) \quad (2)$$

where, n is the number of replications for each combination of factor levels and R is the observed data for each response.

In this case, the smaller the photocatalytic activity is better, which means the noise needs to be minimized and the signal needs to be maximized. Therefore, the lower S/N ratio indicates better performance. Taguchi method is created to reduce the impact of outside influences, such as fluctuations in raw materials or ambient conditions, to strengthen processes and products.

Table 8. Experimental plan and results, and the calculated S/N ratios of Al_2O_3-TiO_2.

Exp. runs	Controllable synthesis parameters			Experimental results		S/N ratios of results
	C	T_h	T_c	Rate constant (R_c)	Rate constant prime (R_c')	
1	1	1	1	0.00614	614	-55.76337
2	1	2	2	0.00453	453	-53.12196
3	1	3	3	0.00251	251	-47.99347
4	2	1	2	0.00281	281	-48.97413
5	2	2	3	0.00119	119	-41.51094
6	2	3	1	0.00304	304	-49.65747
7	3	1	3	0.00232	232	-47.30976
8	3	2	1	0.00551	551	-54.82303
9	3	3	2	**0.00093**	**93**	**-39.36966**

Table 9. Experimental plan and results, and the calculated S/N ratios of SiO_2-TiO_2.

Exp. runs	Controllable synthesis parameters			Experimental results		S/N ratios of results
	C	T_h	T_c	Rate constant (R_c)	Rate constant prime (R_c')	
1	1	1	1	0.03938	3938	-71.90551
2	1	2	2	0.03565	3565	-71.04119
3	1	3	3	0.01167	1167	-61.34142
4	2	1	2	0.03495	3495	-70.86894
5	2	2	3	**0.00557**	**557**	**-54.91710**
6	2	3	1	0.02977	2977	-69.47558
7	3	1	3	0.00633	633	-56.02807
8	3	2	1	0.02359	2359	-67.45456
9	3	3	2	0.00948	948	-59.53617

Besides, the Taguchi method uses a methodical way to carry out tests with a limited number of trials. When compared to conventional experimental design methods, which may call for more experiments, this helps us to save time, resources, and money.

3.3.1 Effect of synthesis parameters on the rate of photodegradation of the hybrid TiO_2 particles

Table 8 and Table 9 show the experimental plan, experimental results, and the calculated S/N ratios of Al_2O_3-TiO_2 and SiO_2-TiO_2. The rate constants were multiplied by 10000 to obtain all S/N ratios with negative values. The higher S/N ratio represents the minimum variation difference between the desirable output and the measured output. The lowest S/N ratios were achieved by A332 (C = 60 mol%, T_h = 145 °C, and T_c = 800 °C) and S223 (C = 50 mol%, T_h = 100 °C, and T_c = 800 °C).

3.3.2 Optimum condition for synthesis of the hybrid TiO_2 particles

Table 10 and Table 11 show the S/N ratio of the hybrid TiO_2 particles, whereas the main effects plot for S/N ratios obtained in the Minitab software tool is shown in Figure 7. The mean S/N ratios were obtained according to the level of the variable, a higher ranking of the variable indicates a greater sensitivity of the system to changes in the parameters. For Al_2O_3-TiO_2 and SiO_2-TiO_2 particles, the highest ranking of the variable was T_c and C, respectively. The lowest ranking of the variables for Al_2O_3-TiO_2 and SiO_2-TiO_2 were C and T_h, respectively. The highest S/N ratios were bolded in both mean S/N ratio response tables of the hybrid TiO_2 particles, which show the predicted optimum synthesis parameters of the samples. For Al_2O_3-TiO_2, it was C = 70 mol%, T_h = 145 °C, and T_c = 900 °C. For SiO_2-TiO_2, it was C = 70 mol%, T_h = 100 °C, and T_c = 900 °C. The predicted optimum process parameters for Al_2O_3-TiO_2 particles were represented by $C_3 - T_{h3} - T_{c3}$, while SiO_2-TiO_2 were represented by $C_3 - T_{h2} - T_{c3}$.

3.3.3 Confirmation test

The hybrid TiO_2 particles were produced by using the predicted optimum synthesis parameters. For example, A333 was produced

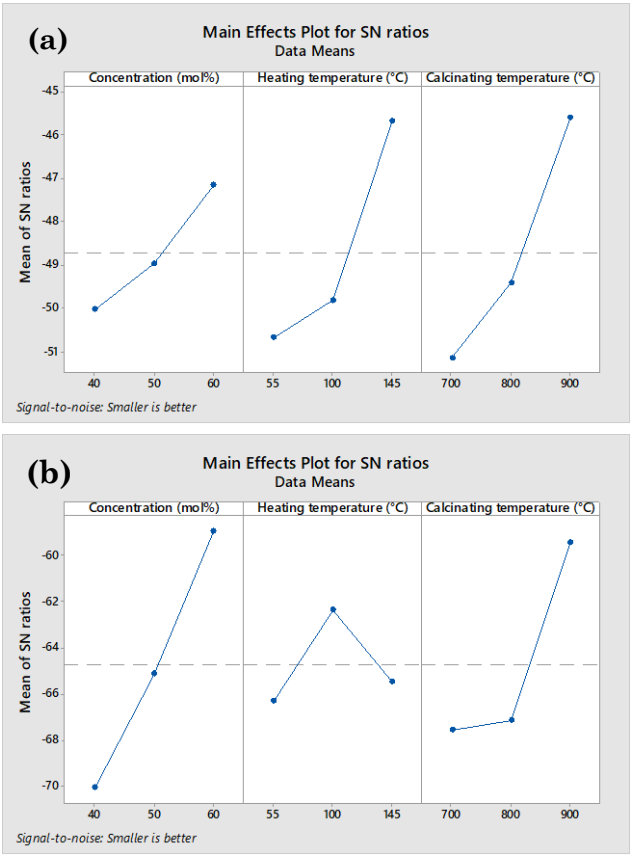

Figure 7. Main effects plot for S/N ratios of (a) Al_2O_3-TiO_2, and (b) SiO_2-TiO_2.

Table 10. Mean S/N ratio response table for Al_2O_3-TiO_2.

Symbol	Synthesis parameters	Mean S/N ratio				
		Level 1	Level 2	Level 3	Max-Min	Rank
C	Concentration of the hybridization materials (mol %)	-50.03	-48.98	**-47.17**	2.86	3
T_h	Heating temperature (°C)	-50.68	-49.82	**-45.67**	5.01	2
T_c	Calcinating temperature (°C)	-51.15	-49.42	**-45.60**	5.55	1

Table 11. Mean S/N ratio response table for SiO_2-TiO_2.

Symbol	Synthesis parameters	Mean S/N ratio				
		Level 1	Level 2	Level 3	Max-Min	Rank
C	Concentration of the hybridization materials (mol %)	-70.08	-65.14	**-58.97**	11.11	1
T_h	Heating temperature (°C)	-66.32	**-62.38**	-67.57	3.95	3
T_c	Calcinating temperature (°C)	-67.57	-67.15	**-59.47**	8.11	2

using the parameters of $C_3 - T_{h3} - T_{c3}$, and S323 was produced using the parameters of $C_3 - T_{h2} - T_{c3}$. Figure 8 shows the UV-Vis absorbance spectra of RhB dye solution degraded by A333 and S323.

To validate the Taguchi predicted optimum synthesis parameters, the predicted S/N ratios (ε_p) were calculated using Equation (3) to estimate and verify the response at predicted optimum synthesis parameters of the hybrid TiO_2 particles [30]. The results of the confirmation tests are shown in Table 12 and Table 13. The experimental S/N ratios were higher than the predicted S/N ratio for both samples. There is a high S/N ratio improvement for both hybrid TiO_2 particles, which were 21.91015 dB and 44.5468 dB respectively compared to the initial synthesis parameters that yielded the lowest rate of photodegradation. It is noted that the removal efficiency of A333 at 90 min was nearly zero, indicating almost 100% photocatalysis suppression. Therefore, the Taguchi predicted optimum synthesis parameters were taken to obtain the best photocatalysis suppression.

$$\varepsilon_p = \varepsilon_1 + \sum_{i=1}^{x}(\varepsilon_0 - \varepsilon_i) \quad (3)$$

where ε_p is the predicted S/N ratio, ε_1 is the mean of total S/N ratio, ε_0 is the mean of S/N ratio at optimum level, and x is the number of input process parameter.

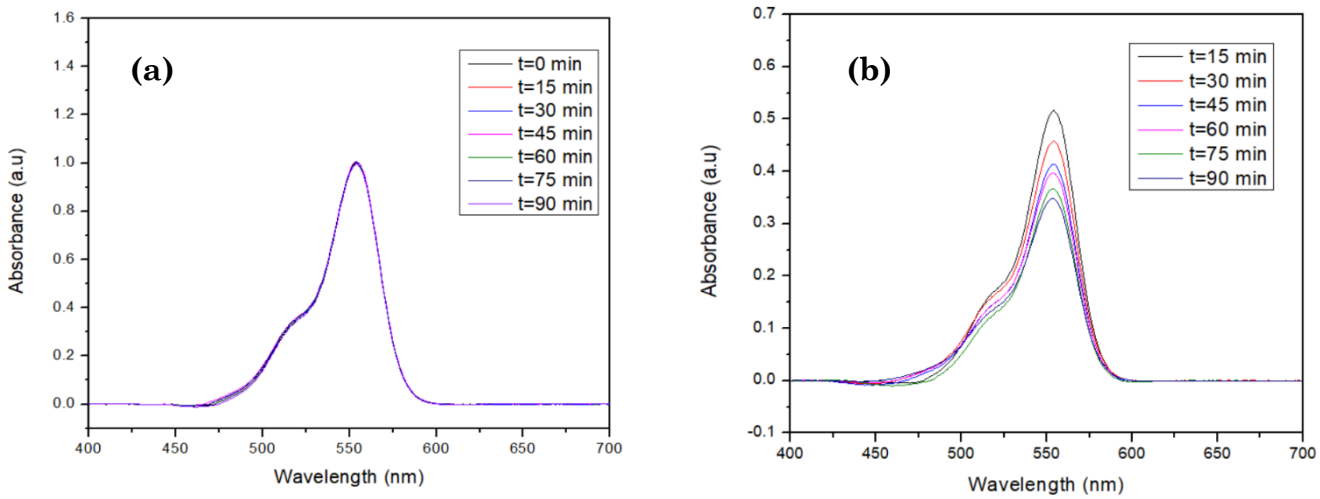

Figure 8. UV-Vis absorbance spectra of RhB solution degraded by (a) A333, and (b) S323.

Table 12. Conformation test results for the rate constant of Al_2O_3-TiO_2.

	Initial synthesis parameter	Optimal synthesis parameters	
		Prediction	Experiment
Level	$C_3 - T_{h3} - T_{c2}$	$C_3 - T_{h3} - T_{c3}$	$C_3 - T_{h3} - T_{c3}$
Rate constant (R_c)	0.00093	-	0.00009
Rate constant prime (R_c')	93	-	9
Removal efficiency at 90 mins (%)	7.49652	-	0.92650
S/N ratio (dB)	-39.36966	-40.99500	-19.08485
Improvement in S/N ratio (dB)	21.91015	-	-

Table 13. Conformation test results for the rate constant of SiO_2-TiO_2.

	Initial synthesis parameter	Optimal synthesis parameters	
		Prediction	Experiment
Level	$C_2 - T_{h2} - T_{c3}$	$C_3 - T_{h3} - T_{c3}$	$C_3 - T_{h3} - T_{c3}$
Rate constant (min^{-1})	0.00557	-	0.00330
Rate constant prime (R_c')	557	-	330
Removal efficiency at 90 min (%)	37.41583	-	21.88500
S/N ratio (dB)	-54.91710	-52.42778	-10.37030
Improvement in S/N ratio (dB)	44.54680	-	-

3.4 Incorporation of Hybrid TiO_2 into Epoxy Thin Film

Table 14 demonstrates the image and yellow index of the epoxy films after irradiation of UV light for 5 h. The degree of yellowing was measured by using the Yellowness Color index measurement of standard Tristimulus values according to the International Commission on Illumination (CIE). The RGB values of the epoxy films were used to calculate the yellowness index of each epoxy thin film using Equation (4) to Equation (7) [42]. The highest value was obtained from the film incorporated by pure TiO_2, followed by no particle incorporated, S323, and A333. It shows that pure TiO_2 increased the degree of yellowing due to the photocatalytic activity that released free radicals which caused the discoloration of epoxy thin film. On the contrary, S323 and A333 reduced the degree of yellowing due to their ability to suppress photocatalytic activity, which reduced the number of free radicals that could degrade the epoxy thin film. Besides, it is believed that S323 and A333 absorbed UV radiation, which further reduced the yellowing of the epoxy thin film caused by UV radiation.

$$X = 0.4125R + 0.3576G + 0.1804B \quad (4)$$

$$Y = 0.2127R + 0.7152G + 0.0722B \quad (5)$$

$$Z = 0.0193R + 0.1192G + 0.9403B \quad (6)$$

where, R is Red values, G is Green values, and B is Blue values.

$$YI = \frac{100\left(C_X X - C_Z Z\right)}{Y} \quad (7)$$

where YI is Yellowness index, C_x is 1.3013, and C_z is 1.1498.

4. Conclusion

Hybrid TiO_2 particles with Al_2O_3 and SiO_2 were synthesized using a sol-gel method and confirmed via the Taguchi L9 orthogonal array to find optimal synthesis parameters by evaluating photodegradation rates in RhB dye solution. The best parameters were C_3–T_{h3}–T_{c3} for Al_2O_3-TiO_2 (A333) and C_3–T_{h2}–T_{c3} for SiO_2-TiO_2 (S323). Confirmation tests showed that A333 and S323 achieved 99% and 75% photocatalytic suppression with S/N ratio improvements of 21.9 dB and 44.6 dB, respectively, using only 21 runs versus 57 required for full factorial design. The photodegradation suppression of A333 shows reduced activity from 0.01305 min^{-1} to 0.00009 min^{-1}, while S323 achieved suppression with photocatalysis activity decreased from 0.01305 min^{-1} to 0.0033 min^{-1}. Particle characterization revealed that A333 had a higher rutile phase (40.1% vs. 10.2% for S323) and a rougher surface, leading to reduced photocatalytic activity compared to S323. XRD, FTIR, FESEM and BET analyses showed that A333's lower surface area and rutile phase contributed to decreased free radical generation. When the optimized hybrid (A333, S323) TiO_2 particles obtained from the Taguchi confirmed test were incorporated into epoxy thin films and UV-irradiated, the yellowness indices were 9.8 for A333, 15.4 for S323, 19.3 for no particles, and 26.5 for pure TiO_2. Thus, A333 and S323 effectively reduced yellowing in epoxy films by suppressing TiO_2 photocatalytic activity.

Table 14. The image and yellow index of the epoxy films after irradiation of UV light.

Particles incorporated	Before UV light	After UV light	RGB values after UV light			Yellowness index
			R	G	B	
None		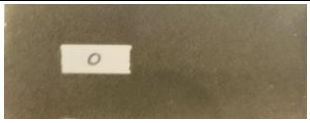	119	106	89	19.2524
Pure TiO_2			200	182	135	26.5291
A333			154	155	136	9.7905
S323	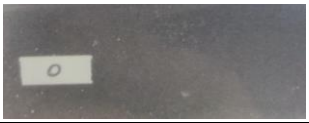		102	97	82	15.3909

Acknowledgement

The authors gratefully acknowledge the financial support of the Ministry of Higher Education Malaysia For the Fundamental Research Grant Scheme With Project Code: FRGS/1/2022/STG05/USM/03/3 and the support from the Universiti Sains Malaysia.

CRediT Authors Statement

Authors Contributions: Sunderishwary S. Muniandy: Conceptualization; Data curation; Formal analysis; Investigation; Methodology; Roles/Writing - original draft. Tan Sek Soon: Conceptualization; Data curation; Formal analysis; Investigation; Methodology; Roles/Writing - original draft. Swee-Yong Pung: Conceptualization; Formal analysis; Funding acquisition; Resources; Validation; Writing - review & editing. Ramakrishnan Sivakumar: Conceptualization; Formal analysis; Investigation; Project administration; Resources; Supervision; Validation; Writing - review & editing. All authors have read and agreed to the published version of the manuscript.

References

[1] Eskandarloo, H., Badiei, A., Behnajady, M.A. (2014). TiO_2/CeO_2 Hybrid photocatalyst with enhanced photocatalytic activity: Optimization of synthesis variables. *Industrial & Engineering Chemistry Research*, 53(19), 7847 – 7855. DOI: 10.1021/ie403460d.

[2] Benčina, M., Iglič, A., Mozetič, M., Junkar, I. (2020). Crystallized TiO_2 nano surfaces in biomedical applications, *Nanomaterials*, 10(6), 1121. DOI: 10.3390/nano10061121.

[3] Ziental, D., Czarczynska-Goslinska, B., Mlynarczyk, D.T., Glowacka-Sobotta, A., Stanisz, B., Goslinski, T., Sobotta, L. (2020). TiO_2 nanoparticles: Prospects and applications in medicine. *Nanomaterials*, 10(2), 387. DOI: 10.3390/nano10020387.

[4] Huang, P., Shi, H.Q., Xiao, H.M., Li, Y.Q., Hu, N., Fu, S.Y. (2017). High performance surface modified TiO_2/silicone nanocomposite. *Scientific Reports*, 7, 5951. DOI: 10.1038/s41598-017-05166-7.

[5] Mont, F.W., Kim, J.K., Schubert, M.F., Schubert, F.E., Siegel, R.W. (2008). High refractive index TiO_2 nanoparticle loaded encapsulants for light-emitting diodes. *Journal of Applied Physics*, 103(8), 083120-083126. DOI: 10.1063/1.2903484.

[6] Trivedi, M., Murase, J. (2017). *Titanium Dioxide in Sunscreen: Application of TiO_2.* London: InTech Open Limited. DOI: 10.5772/intechopen.68886.

[7] Veronovski, N., Verhovšek, D., Godnjavec, J. (2013). The influence of surface-treated nano-TiO_2 (rutile) incorporation in water-based acrylic coatings on wood protection. *Wood Science Technology*, 47(2), 317–328. DOI: 10.1007/s00226-012-0498-3

[8] Yazdan Mehr, J., Lai, X., Li, H., Zeng, X., Zhang, Z. (2018). Synthesis of zirconium-containing polyhedral oligometallasilsesquioxane as an efficient thermal stabilizer for silicone rubber. *Polymers*, 10(5), 520. DOI: 10.3390/polym10050520.

[9] Antunes, A., Popelka, A., Aljarod, O., Hassan, M.K., Luyt, A.S. (2020). Effects of rutile TiO_2 nanoparticles on accelerated weathering degradation of poly (Lactic Acid). *Polymers*, 12(5), 1096. DOI: 10.3390/polym12051096.

[10] Dwyer, D.B., Isbill, S.B., Niedziela, J.L., Kapsimalis, R.J., Duckworth, D.C. (2020). Influence of temperature on accessible pyrolysis pathways of homopolymerized bisphenol A/F epoxies and copolymers. *Journal of Analytical and Applied Pyrolysis*, 153(9), 104978. DOI: 10.1016/j.jaap.2020.104978

[11] Wei, B.X., Zhao, L., Wang, T.J., Gao, H., Wu, H.X., Jin, Y. (2013). Photo-stability of TiO_2 particles coated with several transition metal oxides and its measurement by RhB degradation. *Advanced Powder Technology*, 24(3), 708–713. DOI:10.1016/j.apt.2012.12.009.

[12] Azambre, B., Zenboury, L., Weber, J.V., Burg, P. (2010). Surface characterization of acidic ceria-zirconia prepared by direct sulfation. *Applied Surface Science*, 256(14), 4570-4581. DOI: 10.1016/j.apsusc.2010.02.049

[13] Bouslama, M., Amamra, M.C., Jia, Z., Ben Amar, M., Chhor, K., Brinza, O., Abderrabba, M., Vignes, J.L., Kanaev, A. (2012). Nanoparticulate TiO_2-Al_2O_3 photocatalytic media: Effect of particle size and polymorphism on photocatalytic activity. *ACS Catalysis*, 2(9), 1884-1892. DOI: 10.1021/cs300033y.

[14] Karunakaran, C., Magesan, P., Gomathisankar, P., Vinayagamoorthy, P. (2013). Photocatalytic degradation of dyes by Al_2O_3-TiO_2 and ZrO_2-TiO_2 nanocomposites. *Material Science Forum*. 734, 325–333. DOI: 10.4028/www.scientific.net/MSF.734.325.

[15] Kong, E.D.H., Chau, J.H.F., Lai, C.W., Khe, C.S., Sharma, G., Kumar, A., Siengchin, S., Sanjay, M.R. (2022). GO/TiO_2-related nanocomposites as photocatalysts for pollutant removal in wastewater treatment. *Nanomaterials*, 12(19), 3536. DOI: 10.3390/nano12193536.

[16] Mansour, H., Omri, K., Bargougui, R., Ammar, S. (2020). Novel α-Fe_2O_3/TiO_2 nanocomposites with enhanced photocatalytic activity. *Applied Physics A*, 126, 151. DOI: 10.1007/s00339-020-3320-3.

[17] Tyukavkina, V.V., Shchelokova, E.A., Tsyryatyeva, A.V., Kasikov, A.G. (2021). TiO_2–SiO_2 nanocomposites from technological wastes for self-cleaning cement composition. *Journal of Building Engineering,* 44(46), 102648. DOI: 10.1016/j.jobe.2021.102648.

[18] Xu, L., Shen, Y., Ding, Y., Wang, L. (2018). Superhydrophobic and Ultraviolet-Blocking Cotton Fabrics Based on TiO_2/SiO_2 Composite Nanoparticles. *Journal of Nanoscience and Nanotechnology*, 18(10), 6879–6886. DOI: 10.1166/jnn.2018.15463.

[19] Filatova, E.O., Konashuk, A.S. (2015). Interpretation of the changing the band gap of Al_2O_3 depending on its crystalline form: Connection with different local symmetries. *The Journal of Physical Chemistry C*, 119(35), 20755–20761. DOI: 10.1021/acs.jpcc.5b06843.

[20] Güler, E., Uğur, G., Güler, M. (2020). A theoretical study for the band gap energies of the most common SiO_2 polymorphs. *Chinese Journal of Physics*, 65(1), 472–480. DOI: 10.1016/j.cjph.2020.03.014.

[21] A. Morlando, A., Sencadas, V., Cardillo, D., Konstantinov, K. (2018). Suppression of the photocatalytic activity of TiO_2 nanoparticles encapsulated by chitosan through a spray-drying method with potential for use in sun blocking applications. *Powder Technology*, 329, 252–259. DOI: 10.1016/j.powtec.2018.01.057.

[22] Akshay, V.R., Arun, B., Mandal, G., Mutta, G.R., Chanda, A., Vasundhara, M. (2018). Observation of optical bandgap narrowing and enhanced magnetic moment in co-doped sol-gel-derived anatase TiO_2 nanocrystals. *The Journal of Physical Chemistry C*, 122, 26592–26604. DOI: 10.1021/acs.jpcc.8b06646.

[23] Kaleji, B.K., Gorgani, M. (2022). Comparison of sol-gel and hydrothermal synthesis methods on the structural, optical, and photocatalytic properties of Nb/Ag co-doped TiO_2 mesoporous nanoparticles. *International Journal of Environmental Analytical Chemistry,* 102(14), 3357–3372. DOI: 10.1080/03067319.2020.1767096.

[24] Mekasuwandumrong, O., Pavarajarn, V., Inoue, M., Praserthdam, P. (2006). Preparation and phase transformation behavior of χ-alumina via solvothermal synthesis, *Materials Chemistry and Physics*, 100(2-3), 445–450. DOI: 10.1016/j.matchemphys.2006.01.040.

[25] Siwińska-Stefańska, K., Jesionowski, T. (2017). Advanced hybrid materials based on TiO_2 for Environmental and Electrochemical Applications. In Janus, M., *Titanium Dioxide*. London: InTechOpen Limited. DOI: 10.5772/intechopen.69357.

[26] Liang, Y., Sun, S., Deng, T., Ding, H., Chen, W., Chen, Y. (2018). The preparation of TiO_2 film by the sol-gel method and evaluation of its self-cleaning property. *Materials*, 11(3), 450. DOI: 10.3390/ma11030450.

[27] Lee, H. S., Koo, S. M., Yoo, J. W. (2012). Ceramic processing research TiO_2-SiO_2 nanoparticles for suppressing photocatalytic activities and improving hydrophilicity. *Journal of Ceramic Processing Research,* 13, 300-303.

[28] Lee, M.H., Patil, U.M., Kochuveedu, S.T., Lee, C.S., Kim, D.H. (2012). The Effect of SiO_2 shell on the suppression of photocatalytic activity of TiO_2 and ZnO nanoparticles. *Bulletin of the Korean Chemical Society*, 33(11), 3767–3771. DOI: 10.5012/bkcs.2012.33.11.3767.

[29] Karazi, S.M., Moradi, M., Benyounis, K.Y. (2019). Statistical and Numerical Approaches for Modeling and Optimizing Laser Micromachining Process-Review. In *Reference Module in Materials Science and Materials Engineering*. DOI: 10.1016/B978-0-12-803581-8.11650-9.

[30] Sivaiah, P., Chakradhar, D. (2019). Modelling and optimization of sustainable manufacturing process in machining of 17-4 PH stainless steel. *Measurements*, 134, 142–152. DOI: 10.1016/j.measurement.2018.10.067.

[31] Salim, E.T., Naayi, S.A., Hassan, A.I. (2018). FTIR and XRD analysis of Al_2O_3 nanostructured thin film prepared at low temperature using spray pyrolysis method. *International Journal of Nanoelectronics and Materials,* 11, 1-6.

[32] Zhang, H., Wang, X., Li, N., Xia, J., Meng, Q., Ding, J., Lu, J. (2018). Synthesis and characterization of TiO_2/graphene oxide nanocomposites for photoreduction of heavy metal ions in reverse osmosis concentrate. *RSC Advances*, 8(60), 34241–34251. DOI: 10.1039/C8RA06681G.

[33] Al-Oubidy, E.A., Kadhim, F.J. (2019). Photocatalytic activity of anatase titanium dioxide nanostructures prepared by reactive magnetron sputtering technique. *Optical and Quantum Electronics*, 51(1), 23. DOI: 10.1007/s11082-018-1738-z.

[34] Salim, E.T., Naayi, S.A., Hassan, A.I. (2018). FTIR and XRD analysis of Al_2O_3 nanostructured thin film prepared at low temperature using spray pyrolysis method. *International Journal of Nanoelectronics and Materials*, 11, 1-6.

[35] Praveen, P.V., Iruthagiri, G., Mugundan, S., Shanmugan, N. (2013). Structural, optical, and morphological analyses of pristine TiO_2 nanoparticles synthesized via sol-gel route. *Spectrochimica Acta Part A Molecular and Biomolecular Spectroscopy,* 117, 622–629. DOI: 10.1016/j.saa.2013.09.037.

[36] Madani, M., Omri, K., Fattah, N., Ghorbal, A., Portier, X. (2017). Influence of SiO_2 ratio on structural and optical properties of SiO_2/TiO_2 nanocomposites prepared by simple solid-phase reaction. *Journal of Materials Science: Materials in Electronics*, 28(12), 12977–12983. DOI: 10.1007/s10854-017-7129-6.

[37] Gosens, I., Post, J.A., Fonteyne, L.J., Jansen, E.H.J.M., Geus, J.W., Cassee F.R., Jong, W.H. (2010). Impact of agglomeration state of nano and submicron sized gold particles on pulmonary inflammation. *Particle and Fibre Toxicology,* 7(1), 31. DOI:10.1186/1743-8977-7-37.

[38] Guo, J., Bui, H., Valdesueiro, D., Yuan, S., Liang, B., Ommen, J. (2018). Suppressing the photocatalytic activity of TiO_2 nanoparticles by extremely thin Al_2O_3 films grown by gas-phase deposition at ambient conditions. *Nanomaterials*, 8 (2), 61. DOI: 10.3390/nano8020061.

[39] Bianchi, C., Gatto, S., Pirola, C., Naldoni, A., Di Michele, A., Cerrato, G., Crocellà, V., Capucci, V. (2014). Photocatalytic degradation of acetone, acetaldehyde, and toluene in gas-phase: Comparison between nano and micro-sized TiO_2. *Applied Catalysis B: Environmental*, 146, 123–130. DOI: 10.1016/j.apcatb.2013.02.047.

[40] Cheng, H., Wang, W., Huang, B., Wang, Z., Zhan, J., Qin, X., Zhang, X., Dai, Y. (2013). Tailoring AgI nanoparticles for the assembly of AgI/BiOI hierarchical hybrids with size-dependent photocatalytic activities. *Journal of Materials Chemistry A*, 1(24), 7131–7136. DOI: 10.1039/C3TA10849J.

[41] Hosseini, S., Jahangirian, H., Webster, T.J., Masoudi, S.S., Arou, M.K. (2016). Synthesis, characterization, and performance evaluation of multilayered photoanodes by introducing mesoporous carbon and TiO_2 for humic acid adsorption. *International Journal of Nanomedicine*, 11, 3969–3978. DOI: 10.2147/IJN.S96558.

[42] Eh, C.L.M., Yeo, W.S., Sung, A.N., Abdelrhman, A.N. (2022). Yellowness index measurement model in MATLAB mobile. *AIP Conference Proceedings*, 2676, 020006. DOI: 10.1063/5.0109303.